

# Planets and IR Excesses: Preliminary Results from a *Spitzer*/MIPS Survey of Solar-Type Stars

C. A. Beichman<sup>1</sup>, G. Bryden<sup>1</sup>, G. H. Rieke<sup>2</sup>, J. A. Stansberry<sup>2</sup>, D. E. Trilling<sup>2</sup>, K. R. Stapelfeldt<sup>1</sup>, M. W. Werner<sup>1</sup>, C. W. Engelbracht<sup>2</sup>, M. Blaylock<sup>2</sup>, K. D. Gordon<sup>2</sup>, C. H. Chen<sup>1</sup>, K. Y. L. Su<sup>2</sup>, & D. C. Hines<sup>2</sup>

1) *Jet Propulsion Lab, 4800 Oak Grove Dr, Pasadena, CA 91109*

2) *Steward Observatory, University of Arizona, 933 North Cherry Ave, Tucson, AZ 85721*

## ABSTRACT

As part of a large *Spitzer*/MIPS GTO program, we have searched for infrared excesses due to debris disks toward 26 FGK field stars known from radial velocity (RV) studies to have one or more planets. While none of these stars show excesses at 24  $\mu\text{m}$ , we have detected 70  $\mu\text{m}$  excesses around 6 stars at the 3- $\sigma$  confidence level. The excesses are produced by cool material ( $< 100$  K) located beyond 10 AU, well outside the “habitable zones” of these systems and consistent with the presence of Kuiper Belt analogues with  $\sim 100$  times more emitting surface area than in our own planetary system. These planet-bearing stars are, by selection for RV studies, typically older than 1 Gyr, and the stars identified here with excesses have a median age of 4 Gyr. We find a preliminary correlation of both the frequency and the magnitude of dust emission with the presence of known planets. These are the first stars outside the solar system identified as having both well-confirmed planetary systems and well-confirmed IR excesses.

*Subject headings:* infrared:stars; Kuiper Belt; planetary systems:formation; planetary systems:protoplanetary disks

## 1. Introduction

First discovered by the Infrared Astronomical Satellite (IRAS), the “Vega phenomenon” is characterized by a significant deviation from the expected Rayleigh-Jeans emission of quiescent main-sequence stars (Aumann & Good 1990; Gillett 1986). The excess IR emission from other stars has been attributed to dust orbiting at distances anywhere from less than 1

to more than 100 AU, analogous to the zodiacal cloud and the Kuiper belt in our own solar system. Due to effects such as radiation pressure and Poynting-Robertson drag, the lifetime of the dust is generally much shorter than the age of the system; any dust observed must have been recently produced. In the solar system, dust is generated by collisions between larger bodies in the asteroid and Kuiper belts, as well as from outgassing comets. Extrasolar systems with IR excess presumably have their own supply of large, solid planetesimals and, perhaps, large planets like those in our system.

IRAS found that approximately 15% of main-sequence stars (Plets & Vynckier 1999), predominantly A and F stars, show excesses attributable to dust in orbit around the stars at distances between a few and a few hundred AU and heated by absorbed starlight to temperatures of 30-300 K (Backman & Paresce 1993). Fractional luminosities,  $L_{\text{dust}}/L_{\star}$ , are observed as large as  $10^{-3}$  for stars with bright excesses such as  $\beta$  Pic and as small as  $10^{-5}$  for stars at the detection threshold. These values can be compared to our solar system:  $10^{-8}$  to  $10^{-7}$  for the hot material in the zodiacal cloud (1-3 AU; Dermott et al. 2002) and  $10^{-7}$  to  $10^{-6}$  predicted for the cooler Kuiper Belt region beyond 10 AU (Stern 1996), which is constrained to be  $< 10^{-5}$  by IRAS (Aumann & Good 1990; Teplitz et al. 1999). Observations by the Infrared Space Observatory (ISO; Habing et al. 2001; Spangler et al. 2001) suggest a decline in the fraction of stars with excess IR emission with time, but with the possibility of finding modest ( $L_{\text{dust}}/L_{\star} > 10^{-5}$ ) excesses among older stars (Decin et al. 2000, 2003). *Spitzer* and IRAS results toward more than 200 A stars confirm a general decline in the average amount of emission with little 24  $\mu\text{m}$  emission seen for sources older than 100 Myr but with large variations within each age group studied (Rieke et al. 2004). The variations are probably due in part to sporadic replenishment of dust clouds by individual collisions between large, solid bodies, but also are likely to reflect a range in mass and extent for the initial planetesimal disk.

Images in the optical and near-IR (Heap et al. 2000; Schneider et al. 1999), submillimeter (Holland et al. 1998; Greaves et al. 1998; Holland et al. 2003) and from *Spitzer* itself (Stapelfeldt et al. 2004) have revealed that in some cases the dust exists in flattened disks with warps, gaps, and blob-like structures that have been attributed to the gravitational influence of planets (Wyatt & Dent 2002; Dermott et al. 2002). Still, while the frequency and magnitude of IR excess are strongly correlated with stellar youth, no such correlation has yet been found between IR excess and the presence of planets. Even before the first confirmed discovery of an extrasolar planet orbiting a Sun-like star (51 Peg b; Mayor & Queloz 1995; Marcy & Butler 1995), attempts had been made to find links between planets and dusty debris around other stars (e.g.  $\epsilon$  Eri; Backman & Paresce 1993). While early radial-velocity searches for planets found a planet-like trend for  $\epsilon$  Eridani (Campbell et al. 1988), the candidate planet remains controversial even today due to the extremely high level

of chromospheric activity on this young star. The 7-year periodicity found in the star’s radial velocity (Campbell et al. 1988; Cumming et al. 1999; Hatzes et al. 2000) may be induced by a planet orbiting at several AU (Hatzes et al. 2000) or may instead be a reflection of the star’s poorly understood magnetic cycle. Conversely, 55 Cnc has a well-known planetary system, but claims of a dust disk based on visible imaging (Trilling et al. 2000) and ISO photometry (Dominik et al. 1998) have been ruled out by HST coronagraphy (Schneider et al. 2001), sub-millimeter mapping (Jayawardhana et al. 2002), and *Spitzer*/MIPS measurements presented here. In spite of the many studies specifically designed to find a connection between dust and planets, no systems with both well-confirmed planets and well-confirmed IR excess have yet been observed. In fact, the data to date appear to indicate an anti-correlation between dust and planets (Greaves et al. 2004).

The longstanding assumption that stars besides the Sun might harbor both planets and extended dust emission has still not been verified. The aim of this paper is to use the Multiband Imaging Photometer on the *Spitzer Space Telescope* (MIPS; Rieke et al. 2004) to directly address this outstanding issue by searching for excess IR emission from known planet-bearing stars. MIPS provides unprecedented sensitivity at mid-IR wavelengths and as such is an ideal instrument for searching for the dust emission from solar-type stars. While the focus of this paper is on observations of stars which are known to have planets, for purposes of noise calibration and to greatly improve our statistical analysis, the results for planet-bearing stars are considered within the context of a larger program - the Volume Limited Survey (VLS). VLS is a *Spitzer* GTO program designed to search for excesses around a broad sample of 155 nearby, F5-K5 main-sequence field stars, sampling wavelengths from 8-40  $\mu\text{m}$  with IRS and 24 & 70  $\mu\text{m}$  with MIPS. This survey consists of two components - stars with planets and those without. The stars without known planets represent a true volume-limited sample selected for expected 70  $\mu\text{m}$  brightness and low levels of infrared cirrus. The sample includes G and late F stars out to 25 pc and early K stars out to 15 pc. This component of VLS consists of 114 stars (without planets), 58 of which have already been observed. These stars will be discussed in more detail in a separate paper (Bryden et al. 2005); here we focus on the second component of the VLS program - planet-bearing stars. The planet-bearing sample was selected from a group of stars of similar spectral types known to have RV planets. Of 41 planned targets, 26 have been observed to date. These stars are not necessarily located in regions of low infrared cirrus and are typically farther away ( $\sim$ 15-50 pc) than the non-planet VLS sample. It is worth noting that the disk around  $\epsilon$  Eri, a K0 star located 3.3 pc away, would have been undetectable by IRAS if that star were located even 10 pc away; its 60  $\mu\text{m}$  flux density would then have dropped below the completeness limit of the Faint Source Catalog (Moshir et al. 1990). The sensitivity of *Spitzer*/MIPS allows the search for disks not just around the nearest FGK stars, but also around those

located at distances of 10-50 pc around which planets have been identified.

We present our MIPS observation in §2, along with a full error analysis to determine whether any measured excesses are statistically significant. For the systems with IR excess, §3 attempts to find a correlation with system parameters such as stellar metallicity/age or planet mass/semi-major axis. Before the concluding remarks (§5), we describe how our MIPS observations constrain the dust properties in each system (§4).

## 2. Observations

During its first year of operation *Spitzer* observed from the VLS sample 26 stars with RV planets (Table 1) and an additional 58 stars without any known planets. All stars were observed at 70  $\mu\text{m}$ . One planet-bearing star, HD128311, was not observed at 24  $\mu\text{m}$  due to scheduling constraints, but its spectrum at this wavelength was measured with IRS Long-Low and was found to be consistent with no excess shortward of 30  $\mu\text{m}$ . The remainder of the planet-bearing stars were observed at 24  $\mu\text{m}$  and detected with high signal-to-noise ratio (SNR).

### 2.1. Data Reduction

Our data reduction is based on the DAT software developed by the MIPS instrument team (Gordon et al. 2004a). Because the data pipeline is still under development and the adopted calibration numbers are likely to change with further improvements in the overall MIPS data analysis, we list our chosen set of data reduction parameters in detail.

For each of the 24  $\mu\text{m}$  and 70  $\mu\text{m}$  bands, the instrument calibration was derived from  $\sim 75$  observations of  $\sim 35$  different stars. To minimize systematic uncertainties, a mix of stellar types was used: most of the calibrators are K giants, several are A stars, and a few are solar analogs. The 24  $\mu\text{m}$  photosphere predictions were derived from stellar templates (e.g. Cohen et al. 1999) for K giants, from Kurucz models (e.g. Kurucz 2003) for A stars, and from the solar spectrum (e.g. Tobiska et al. 2000) for the solar analogs. The 70  $\mu\text{m}$  photospheric predictions were obtained similarly, except that the analytic spectral functions of Engelke (1992) were used to extrapolate the K giant templates out to 70  $\mu\text{m}$ .

At 24  $\mu\text{m}$ , we carried out aperture photometry on reduced images using an aperture 6 camera pixels (1 pixel=2.5'' at 24  $\mu\text{m}$ ) in radius, a background annulus from 12 to 17 pixels, and an aperture correction of 1.15. The flux level is calibrated at 1.047  $\mu\text{Jy}/\text{arcsec}^2/(\text{DN}/\text{s})$ , with a default color correction of 1.00 appropriate for sources warmer than 4000 K at a

weighted-average wavelength of  $23.68 \mu\text{m}$ . Final images were mosaiced from individual frames with quarter-pixel subsampling.

At  $70 \mu\text{m}$  we used images processed beyond the standard DAT software in order to correct for time-dependent transients, corrections which can significantly improve the sensitivity of the measurements (Gordon et al. 2004b). At  $24 \mu\text{m}$ , a large enough aperture was chosen so as to integrate all of the flux out to roughly the first Airy ring. Because the accuracy of the  $70 \mu\text{m}$  data is limited by background noise, rather than instrumental effects, such a large aperture contains an undesirable amount of sky fluctuations. In order to maximize signal-to-noise, a smaller aperture is more appropriate at  $70 \mu\text{m}$  - just 1.5 pixels in radius. With a 4 to 8 pixel radius sky annulus, this aperture size requires a relatively high aperture correction of 1.79. The flux level is calibrated at  $15,800 \mu\text{Jy}/\text{arcsec}^2/\text{MIPS}_{70}\text{unit}$ , again with a default color correction of 1.00 (MIPS<sub>70</sub> units are based on the ratio of the measured signal to the stimulator flash signal). Images were mosaiced from individual frames with half-pixel subsampling. For both the  $24 \mu\text{m}$  and  $70 \mu\text{m}$  data, neighboring point sources were subtracted from the images before measuring the sky brightness. Also for both wavelengths, we fix each target’s position, rather than centroid onto the peak of the local flux distribution. If the target position is not fixed, the centroid position tends to float toward any local noise fluctuations, resulting in an inappropriately high flux measurement, particularly for noisy fields. The fact that no centering of the aperture is required is a reflection of the excellent telescope pointing intrinsic to *Spitzer* ( $<1''$ ; Werner et al. 2004).

In order to determine whether any of our target stars have an IR excess, we compare the measured photometry to predicted photospheric levels. For convenience in extrapolating the photospheric emission we have fitted Kurucz models (Castelli 2003; Kurucz 2003) to a combination of short wavelength data taken primarily from the Tycho/Hipparcos (visible), Johnson (bright near-IR) or 2MASS (faint near-IR), and IRAS ( $12 \mu\text{m}$ ) catalogs. After excluding one outlying point for a star with an excess (HD69830, which will be discussed elsewhere; Beichman et al. 2005), the 83 flux measurements at  $24 \mu\text{m}$  have an average  $F_{\text{MIPS}}/F_{\text{photosphere}}$  of 0.99 which, although gratifyingly close to unity, is not surprising given that the present *Spitzer* calibration is based on similar stellar models. More importantly for our purposes, the dispersion of  $F_{\text{MIPS}}/F_{\text{photosphere}}$  is 0.07 for this sample (Fig. 1).

At  $70 \mu\text{m}$ , 73 out of 84 stars (both planet-bearing and without planets) are detected with signal-to-noise ratio  $> 3$ . This is in contrast with previous IR surveys of AFGK stars with ISO, in which only half of the stars without excess were detected (Habing et al. 2001). While the sensitivity of these *Spitzer* observations is roughly a factor of 10 better than previous data, *Spitzer*’s sensitivity is limited by extragalactic source confusion and cirrus (see below) which will make it difficult to look for excesses around stars much fainter than

those discussed here.

The distribution of 70  $\mu\text{m}$  flux densities relative to the expected photospheric values is shown in Fig. 2. Unlike the tight distribution of flux ratios at 24  $\mu\text{m}$ , several stars have 70  $\mu\text{m}$  flux much higher than expected from the stellar photosphere alone. In one case, the 70  $\mu\text{m}$  flux is high by a factor of 15. Many of the stars (12) will be identified in the following as having statistically significant IR excess. Ignoring these stars with excesses and those with  $\text{SNR} < 3$ , the average ratio of MIPS flux to predicted photosphere is  $|F_{\text{MIPS}}/F_{\text{photosphere}}| = 1.03 \pm 0.04$ , consistent with the present calibration. More important than the absolute calibration of  $F_{\text{MIPS}}/F_{\text{photosphere}}$  is its dispersion, which indicates the overall accuracy of the flux measurements and gives an immediate sense of the minimum level of excess necessary for detection. The dispersion in the 70  $\mu\text{m}$  sample is 28% (excluding the stars with excesses), considerably higher than that in the 24  $\mu\text{m}$  data (7%). The following section (§2.2) discusses in more detail the noise levels within the 70  $\mu\text{m}$  data.

Fig. 3 shows the spectral energy distributions for two of the planet-bearing stars, HD82943 and HD117176, that have excess 70  $\mu\text{m}$  emission. Published photometric fluxes for these stars from visible to infrared are well fit by Kurucz stellar atmospheres (dotted lines; Castelli 2003; Kurucz 2003). The *Spitzer*/MIPS 24  $\mu\text{m}$  fluxes are also well fit by the model atmospheres (within 1% for HD82943, 5% low for HD117176). The 70  $\mu\text{m}$  emission, meanwhile, is well above that expected from the stellar photosphere alone; an additional component of emission due to dust must be added to the Kurucz model in order to fit the 70  $\mu\text{m}$  data. Because there is only a single 70  $\mu\text{m}$  measurement of IR excess, however, the SED can be fit by a range of dust temperatures and luminosities. Constraints on the dust in these systems are discussed in §4.

## 2.2. Detection of Excess at 70 $\mu\text{m}$

A potential correlation of planets with IR excess is already apparent in Fig. 2, in which 4 of the 5 largest 70  $\mu\text{m}$  flux ratios are for stars which harbor planets, even though planet-bearing stars make up less than one-third of the sample. Still, without a proper analysis of the noise levels in each field it is impossible to assess whether the IR excesses are statistically significant.

In general, the sources of noise can be divided into pixel-to-pixel noise (which we refer to as “sky” noise) and errors for the field as a whole (“systematic” noise). The pixel-to-pixel noise is a combination of detector/photon noise along with real sky background fluctuations. For the 24  $\mu\text{m}$  measurements, photon noise is negligible. Even with the minimum allowed

integration time (1 cycle of 3 sec exposures = 48 sec), the sensitivity of MIPS is overwhelming; even our dimmest source could theoretically be detected in just a few milliseconds. Further, the background noise is low: galactic cirrus is weak at this wavelength; the zodiacal emission is relatively smooth across the field of view; and the confusion limit for distant extragalactic sources is just 0.056 mJy (Dole et al. 2004b).

Instead, for the 24  $\mu\text{m}$  measurements, systematic errors dominate. The instrumental contribution to these errors is thought to be very low: 24  $\mu\text{m}$  observations of calibrator stars are stable with 1% rms deviations over several months of observations (Rieke et al. 2004). In addition to any residual instrumental problems, the dispersion in  $F_{\text{MIPS}}/F_{\text{photosphere}}$  can include errors in the photosphere extrapolation and the effects of source variability. The fitting of the photosphere can be as precise as 2% when the best 2MASS  $K_s$  photometry is available (Skrutskie et al. 2000), but for stars brighter than  $K_s < 6$  mag, 2MASS data are less accurate and lower precision near-IR data and/or shorter wavelength observations must be used. Extrapolation from visible data places considerably more weight on the photospheric models and may result in greater uncertainty in the predicted photospheric levels at 24  $\mu\text{m}$  and 70  $\mu\text{m}$ .

While the relative contributions of instrumental and fitting errors to the 24  $\mu\text{m}$  dispersion are unknown, it is clear that the photometry is currently limited to 7% accuracy due to their combined effects. While this may improve with further instrument analysis and better photospheric models, 3- $\sigma$  detections of excess at 24  $\mu\text{m}$  now require measured fluxes at least 20% above the stellar photosphere. Only one of our sources (HD69830) meets this requirement, with a strongly significant 45% excess. The relatively hot dust emission in this system, which is not yet known to have any planets, will be discussed in a separate paper (Beichman et al. 2005).

At 70  $\mu\text{m}$  we planned the number of observing cycles (each with 126 sec integration time) so that the expected detector/photon noise would be  $\sim 0.1$  of the stellar flux, or equivalently, to achieve a signal-to-noise (SNR)  $\sim 10$  on the stellar photosphere. Integration times range from a few minutes up to 1 hour. Within each reduced image, we estimate the sky noise by directly measuring the standard deviation in the background flux when convolved with our chosen aperture size. Based on this measured sky noise, we find a median SNR of  $\sim 6$ , excluding the sources identified as having an excess. This noise estimate, however, includes contributions beyond just detector/photon noise. Unlike at 24  $\mu\text{m}$ , the fluctuations in the background at 70  $\mu\text{m}$  can be significant. This background, a combination of galactic cirrus and extragalactic confusion, creates a noise floor for each field which cannot be improved with increased integration time. To try to minimize this problem, the target stars in the Volume Limited Sample came from areas of low galactic cirrus, as estimated from the IRAS

Sky Survey Atlas (IPAC 1994). The confusion limit for extragalactic background sources, however, is unavoidable and sets a strict lower limit for the sky noise at  $70\ \mu\text{m}$ . Dole et al. (2004b) find a  $5\text{-}\sigma$  confusion limit of 3.2 mJy based on source counts from *Spitzer* (Dole et al. 2004a) extrapolated to fainter fluxes with the model of Lagache et al. (2004). In our sample, the lowest ( $1\text{-}\sigma$ ) noise levels observed toward stars located in clean portions of the sky are  $\sim 2$  mJy, somewhat worse than Dole et al.’s best-case limit. This difference is attributable to the larger effective beam size used for our photometry/noise calculations. On top of the confusion limit, a few sources have higher noise values due to galactic cirrus and/or modestly worse than typical detector performance. In particular, HD168443, located within 2.5 degrees of the galactic plane, shows extremely high levels of cirrus noise (30 mJy/aperture, approximately equal to the level predicted from the IRAS Sky Survey Atlas) and is not considered further.

While we can directly examine the overall background noise in each of our  $70\ \mu\text{m}$  images, the systematic error terms are more difficult to evaluate. These errors must certainly be as large as those in the  $24\ \mu\text{m}$  data since the photospheric fitting errors should be the same for both wavelengths. Within our data, we find that the observed dispersion of fluxes at  $70\ \mu\text{m}$  is consistent with larger systematic errors than at  $24\ \mu\text{m}$ . We assume that the systematic errors in the  $70\ \mu\text{m}$  data are 15% of the stellar flux, about twice the dispersion in the  $24\ \mu\text{m}$  data. Given the complex calibration required for the  $70\ \mu\text{m}$  Germanium photoconductors, this is an excellent level of performance.

Adding all of the noise sources (photon noise, sky background, model fitting, and residual calibration issues) together in quadrature gives us a final noise estimate for each  $70\ \mu\text{m}$  target. In Table 2 we list these noise levels, along with the measured and the photospheric fluxes, for each of the planet-bearing stars. We use these noise estimates to calculate  $\chi_{70}$ , the statistical significance of any IR excess

$$\chi_{70} \equiv \frac{F_{70} - F_{\star}}{N_{70}} \quad (1)$$

where  $F_{70}$  is the measured flux,  $F_{\star}$  is the expected stellar flux, and  $N_{70}$  is the noise level, all at  $70\ \mu\text{m}$ . The resultant histogram is shown in Fig. 4. Based on this criterion, we find that 6 out of 25 planet-bearing stars have a  $3\text{-}\sigma$  or greater excess at  $70\ \mu\text{m}$ : HD33636 (BD+04858), HD50554 (BD+241451), HD52265 (HR2622), HD82943, HD117176 (70 Vir), and HD128311 (GJ3860). Of the remaining stars,  $3\text{-}\sigma$  upper limits on any excess flux range from 0.1 to 1.9 times the stellar flux, with a median of upper limit of  $0.7 F_{\star}$ . The focus of this paper is the planet-bearing stars; the non-planet stars with excess will be discussed in a separate paper on the Volume Limited Sample (Bryden et al. 2005).

Fig. 5 shows the  $70\ \mu\text{m}$  images for each of the six planet-bearing stars identified as having significant  $70\ \mu\text{m}$  excess. The full-width half-maximum for the telescope’s point spread



function at  $70\ \mu\text{m}$  is  $17''$ ; there is no evidence for any emission extended beyond the point spread function. The background noise fluctuations are generally smooth across the field, with the exception of HD52265 which has obvious cirrus contamination concentrated toward the NW corner of the image. Within the entire  $\sim 5 \times 2.5$  arcmin MIPS field of view, most of the images contain point sources other than the target star. Some of these neighboring sources have corresponding  $24\ \mu\text{m}$  emission, while others are only detected at  $70\ \mu\text{m}$ .

### 2.3. Notes on individual sources

*HD82943*: This is our strongest detection of an excess, with a  $70\ \mu\text{m}$  flux 15 times the stellar photosphere. The lack of excess at  $24\ \mu\text{m}$  requires the spectral energy distribution to rise steeply above the photosphere between  $24$  and  $70\ \mu\text{m}$ . As the brightest excess detection (113 mJy), this is the most promising candidate for follow-up detection at longer IR and sub-mm wavelengths. We also note that the claimed detection of  ${}^6\text{Li}$  in this star's atmosphere could be explained by the accretion of several  $M_{\oplus}$  of rock (Israelian et al. 2001, 2003). While our observed IR excess implies that collisions could have recently showered the star with some solid material, it is not clear whether the magnitude of this accretion is large enough to account for the enhanced lithium abundance.

*HD33636 & HD50554*: These similar stars both have considerable excess at  $70\ \mu\text{m}$  ( $\sim 7$  times the stellar flux), but still only emit 33 and 40 mJy respectively. Although dim, these systems may still be detectable at sub-mm wavelength if the dust is cold enough ( $\lesssim 40$  K), and even upper limits at longer wavelengths would greatly help to constrain the dust temperature, and hence location.

*HD128311*: This star shows a definite detection above the photospheric level at  $70\ \mu\text{m}$ , but a high degree of galactic cirrus and/or anomalous instrument artifacts make follow-up observations important for determining the strength of the excess more accurately. The *Spitzer*/IRS spectrum for this source lies well below the low quality (FQUAL=2) detection at  $25\ \mu\text{m}$  by IRAS and shows no evidence for an excess out to  $30\ \mu\text{m}$ . Additional photometric measurements with MIPS are currently scheduled.

*HD117176 (70 Vir)*: Unlike all of our other stars with  $70\ \mu\text{m}$  excess, the accuracy of the flux measurements for this star are limited by systematic/fitting errors, rather than by sky noise. Additional work to determine the source of the systematic errors will help quantify the overall noise level for this star.

*HD52265*: Although this star has a high level of excess at  $70\ \mu\text{m}$  (a factor of 4 above the stellar photosphere), this is our least statistically significant detection of excess due to

a high level of galactic cirrus in the field. This noise (7.4 mJy) unfortunately may not be greatly reduced with additional integration time. Interestingly, this star happens to fall in the limited field of view of the future space-based telescope COROT (Baglin et al. 2002). As the only planet-bearing primary target for that mission, its visible emission will be monitored over an extended time period for any variability due to transiting objects.

*HD142*: This star has a flux twice that of the stellar photosphere, but the potential excess is only significant at the  $2.4\text{-}\sigma$  level. A relatively short integration time was used (3 cycles) resulting in above average background noise. Additional follow-up observations of this star should clarify whether the excess is due to dust or is just a noise fluctuation.

*55 ( $\rho$ ) Cnc*: With a measured flux of  $18.9 \pm 3.8$  mJy (compared to a predicted stellar flux of 18.2 mJy), we find no evidence for an IR excess. This is in contrast with a claimed detection of 60  $\mu\text{m}$  excess by ISO (Dominik et al. 1998) at the level of  $170 \pm 30$  mJy. The original detection has more recently been attributed to background extragalactic sources based on sub-mm mapping of the region (Jayawardhana et al. 2002). We confirm the presence of two (presumably) extragalactic 70  $\mu\text{m}$  sources located at 08:52:37+28:20:05 and 08:52:35+28:19:18, which correspond to sub-mm sources 1 and 3 from Jayawardhana et al. (2002). However, the 70  $\mu\text{m}$  flux from these neighboring sources is small; a beam large enough to enclose them makes little appreciable change in the total integrated flux.

*$\rho$  CrB & HD210277*: Along with 55 Cnc, these stars were identified as having extended emission via coronagraphic measurements at visible wavelengths (Trilling et al. 2000). We find no evidence for excess emission around either star at 24 or 70  $\mu\text{m}$ .

### 3. Correlation of Excess with System Parameters

Here we examine whether IR excess is correlated with stellar properties (age, metallicity, spectral type) and planet orbital characteristics (planet mass, semi-major axis, eccentricity). The planet and star properties are summarized in Tables 1 and 3.

The planetary systems considered here all have at least one planet with mass greater than Jupiter's and with semi-major axis smaller than Jupiter's. Considering this sample in aggregate, there is a clear trend between the presence of this type of planet and the detection of IR excess. Within our sample we have found 6 stars with excesses out of the 25 planet-bearing stars for a detection rate of  $24 \pm 10\%$ . This is much less than the excess detection rates for young stars; Habing et al. (2001) observe that 60% of A-K stars younger than 400 Myr have excess 60  $\mu\text{m}$  emission, while Rieke et al. (2004) similarly find that half of young A stars have excess 24  $\mu\text{m}$  emission. Analysis of IRAS and ISO data suggests that the

fraction of stars with excesses drops considerably with increasing age, however, particularly beyond 1 Gyr (Habing et al. 2001; Decin et al. 2003). The nominal IRAS statistics suggest that excesses are found around just 10-15% of all main-sequence stars (Backman & Paresce 1993), a factor of two less than our detection rate. If ages older than 1 Gyr are considered, the disparity in rates becomes more significant. ISO surveys found excesses around only  $10 \pm 3\%$  of stars older than 400 Myr (Decin et al. 2000; Habing et al. 2001). This detection rate is similar to that found within our sample of stars not known to have planets (Bryden et al. 2005). Within this group,  $10 \pm 4\%$  (6 out of 58) of the stars exhibit excess IR emission at  $70 \mu\text{m}$ . Among stars older than 1 Gyr, the detection rate for stars with planets is more than double that for stars without. This tentative result would be consistent with the suggestion of Dominik & Decin (2003) that excesses due to Kuiper Belt material can have very long lifetimes. The apparent increase in frequency of dust disks around planet-bearing stars over stars without known planets implies that searches for dust disks might benefit from targeted searches of planet-bearing stars. The converse would also be true - planet searches, via radial velocity or otherwise, may benefit from specifically targeting stars with IR excesses. This correlation is preliminary and will be examined closely as additional stars in this survey are observed.

### 3.1. Planet Orbital Characteristics

What kind of planets do stars with debris disks possess? Table 1 and Fig. 6 summarize the properties of the planetary systems. Two of the systems with strong excesses have large planets on distant, eccentric orbits ( $9.3 M_{\text{Jup}}$  at 3.6 AU for HD33636 and  $4.9 M_{\text{Jup}}$  at 2.4 AU for HD50554). The system with strongest excess, HD82943, has two moderate-sized planets with masses  $\sim 1 M_{\text{Jup}}$  at 0.73 and 1.16 AU. Overall, however, the distribution of planets associated with IR excess is little different than for those without an excess. For every type of planet with IR excess, there are counter-examples without excess: for example, HD39091 has a large planet on a distant, eccentric orbit yet shows no dust emission. The only possible trend is that no systems with short-period planets ( $< 0.25$  AU) exhibit any IR excess, though the small-number statistics limit the strength of this conclusion.

Planets should affect the diffuse material in their immediate vicinity. The region under the direct gravitational influence of a planet at  $a_p$  with eccentricity  $e_p$  has a half-width of  $\sqrt{4e_p^2 a_p^2 / 3 + 12r_H^2}$ , where  $r_H \equiv a_p (M_p / 3M_\star)^{1/3}$  is the Hill radius (e.g. Bryden et al. 2000). For the planet orbiting HD33636 ( $M_p \sin i = 9.28 M_{\text{Jup}}$ ,  $a_p = 3.56$  AU,  $e_p = 0.53$ ) this directly perturbed region extends from 1 to 6 AU where we have ignored the unknown inclination effect which enters only weakly into the Hill radius. This zone would be cleared of any large

objects that might provide a local source of dust generation. Although dust could drift toward the planet from a distant belt of source bodies, Jupiter-mass planets are efficient at gravitationally scattering this dust from their neighborhood (Moro-Martin & Malhotra 2005). Outside of the planet’s region of direct influence, substantial Kuiper Belt material could be present at distances  $\gtrsim 10$  AU and effective temperatures below 100 K, consistent with the cool excess (no 24  $\mu\text{m}$  emission) seen toward these stars. Additional *Spitzer* and ground-based submillimeter data are required to constrain the temperature and the physical distribution of this material (Sheret et al. 2004).

### 3.2. Stellar Properties

Stellar ages cited in the literature for these stars span at least a factor of two, highlighting the difficulty in determining ages for mature, main sequence stars. Whenever possible, we adopt ages from the compilation of Wright et al. (2004) which provides a uniform tabulation for 1200 stars based on Ca II H&K line strengths. While Table 3 lists the ages for the planet-bearing stars, Fig. 7 gives a histogram for the larger sample, both with and without planets.

There is no obvious age difference between the overall planet-bearing and non-planet bearing samples; their median ages are 6 and 4 Gyr respectively. The one outlier among the planet-bearing sample is HD128311, which has no well-determined age. It is listed as a possible member of the UMa moving group (King et al. 2003) based on its chromospheric activity and its X-ray detection in the ROSAT All Sky Survey. Both of these indicators suggest an age of 0.5-1 Gyr. In Fig. 7, the stars with excess are flagged with arrows, solid for planet-bearing stars and open for those without. With the exception of HD128311, the planet-bearing stars with excesses are all much older than a billion years. The planet-bearing excess stars are slightly younger than the planet-bearing sample as a whole (4.4 vs. 6.0 Gyr), but the difference is not statistically significant. Any inverse correlation of age with amount of dust is much weaker than that observed in stars younger than 1 Gyr (e.g. Decin et al. 2003; Rieke et al. 2004).

Fig. 8 presents a similar histogram for the metallicity of stars with/without planets, again marking IR excess stars with arrows. The distribution of metallicities for planet-bearing stars (dark grey) is clearly different than for those without planets (light grey). The typical metallicity of stars with planets is well known to be greater than solar (Wright et al. 2004; Fischer & Valenti 2003) so the fact that the average metallicity of these stars is slightly greater than solar,  $[\text{Fe}/\text{H}] = 0.13 \pm 0.05$  with a dispersion of 0.19, is no surprise. Although the planet-bearing stars with excess have an average metallicity above solar, their

average  $[\text{Fe}/\text{H}]=0.05$  is below the planet-bearing average. Comparing the stars with and without planets to their own samples, there is no evidence for higher metallicity resulting in a greater amount of IR emitting dust.

#### 4. Analysis of Detected Dust

Unfortunately, our detections of IR excess provide only limited information about the properties of the dust in each system. Ideally, we would like to determine the dust’s temperature, mass, grain sizes, and overall distribution. Because none of our sources are resolved (see Fig. 5), we have no information on whether the dust disk has any asymmetric structure such as a warp, a centering offset, or general clumpiness. Still, we can use the spectral energy distribution (SED) to provide some constraints on the dust properties. The most direct constraint provided by the SED is on the dust temperature, which then can be converted into a radial distance from the central star. As seen in Fig. 3,  $24\ \mu\text{m}$  measurements provide an upper limit on the dust temperature, while sub-mm limits set a lower limit. Because we usually have no information longward of  $70\ \mu\text{m}$ , however, only an upper limit on the temperature (or an inner limit on the dust’s orbital location) can be derived. If a dust temperature is assumed, the observed flux can be translated into the total dust disk luminosity relative to its parent star.

For disks with detections of IR excess, a minimum dust luminosity can be calculated. Using the blackbody formula for flux ( $F \propto L/T^4(e^{h\nu/kT} - 1)$ ), for long wavelength radiation (i.e. on the Rayleigh-Jeans tail of the stellar blackbody curve), the ratio of dust to stellar fluxes becomes

$$\frac{F_{\text{dust}}}{F_{\star}} = \frac{L_{\text{dust}}}{L_{\star}} \frac{h\nu T_{\star}^3}{kT_{\text{dust}}^4 (e^{h\nu/kT_{\text{dust}}} - 1)} \quad (2)$$

The minimum disk luminosity as a function of  $70\ \mu\text{m}$  dust flux can be obtained unambiguously by setting the emission peak at  $70\ \mu\text{m}$  (or, equivalently,  $T_{\text{dust}} = 52.5\text{K}$ ) :

$$\frac{L_{\text{dust}}}{L_{\star}}(\text{minimum}) = 10^{-5} \left( \frac{5600\ \text{K}}{T_{\star}} \right)^3 \frac{F_{70,\text{dust}}}{F_{70,\star}} \quad (3)$$

Consistent with this formula, Fig. 9 shows constraints on  $L_{\text{dust}}/L_{\star}$  and  $T_{\text{dust}}$  for HD82943, the planet-bearing star with  $70\ \mu\text{m}$  flux a factor of 15 above the stellar photosphere. The lines in this figure are based on the  $3\text{-}\sigma$  limits to the observed  $24$  and  $70\ \mu\text{m}$  fluxes.  $T_{\text{dust}}$  is meant to signify the typical emitting temperature for the dust; in reality some range of temperatures will be found in any given system. For this star, our strongest detected excess, the minimum  $L_{\text{dust}}/L_{\star}$  is relatively high -  $1.4 \times 10^{-4}$  - more than two orders of magnitude

above estimates for the Kuiper belt’s luminosity. (A listing of minimum  $L_{\text{dust}}/L_{\star}$  for the other planet-bearing stars is given in Table 2.) The dust temperature is well-constrained by the lack of  $24 \mu\text{m}$  excess to be  $\lesssim 70$  K at the  $3\text{-}\sigma$  level (the cross-hatched region in Fig. 9) or  $\lesssim 60$  K at the  $1\text{-}\sigma$  level (the solid-filled region). Dust at lower temperatures showing greater emission at longer wavelengths cannot be ruled out.

Sub-mm observations are critical to constraining the dust properties and thus the overall mass of the material responsible for the excess in these stars. Fig. 10 shows the limits on the dust characteristics for a case where sub-mm data is available to help constrain the dust temperature on the low end. (Greaves et al. (2004) observed HD117176 at  $850 \mu\text{m}$ , measuring a flux of  $2.3 \pm 2.4$  mJy.) Note that in order to set the most strict limits, we assume that the grains are small enough that their emissivity drops off as  $\lambda^{-2}$  for long-wavelength radiation (see e.g. Draine & Lee 1984; Wyatt & Dent 2002). The sub-mm measurement does set a lower limit for the dust temperature, but because the  $70 \mu\text{m}$  emission is not as strong as for the previous star, the upper limit on temperature is less strict. Overall, the possible range of dust temperature and luminosity are much better constrained:  $1\text{-}\sigma$  limits (the solid-filled region in Fig. 10) give  $T_{\text{dust}} \approx 20$  to  $100$  K,  $L_{\text{dust}}/L_{\star} \approx 10^{-5.2}$  to  $10^{-4.2}$ . For a temperature of  $50$  K, this disk brightness corresponds to a total dust surface area of  $\sim 10^{25}\text{-}10^{26}$   $\text{cm}^2$  or, equivalently, a dust mass of  $\sim 10^{-6}\text{-}10^{-5}M_{\oplus}$  in  $100 \mu\text{m}$  grains. The mass contained in larger planetesimals is even less certain.

For stars with no detected emission, a  $3\text{-}\sigma$  upper limit on the fluxes leads to upper limits for  $L_{\text{dust}}/L_{\star}$  of  $10^{-6}$  to  $10^{-5}$ , assuming a dust temperature of  $\sim 50$  K (again see Table 2). For these stars we are setting limits of  $\sim 10\text{-}100$  times the level of dust in our solar system. Deeper integrations on these stars may result in detections of fainter excesses or improved upper limits, but extragalactic confusion or cirrus will set limits on the amount of detectable excess for these relatively distant stars. Non-planet bearing stars in the VLS are brighter and typically located in more cirrus-free regions, so that our  $L_{\text{dust}}/L_{\star}$  limits for these objects tend to be more sensitive than for the planet-bearing stars reported here.

## 5. Conclusions

*Spitzer*/MIPS observations of 26 main-sequence FGK stars which are known to have planetary companions reveal  $70 \mu\text{m}$  dust emission from 6 debris disks. These are the first examples outside the solar system of stars which have both well-confirmed planets and well-confirmed IR excesses. We conclude from this study that excesses at  $70 \mu\text{m}$  are at least as common around planet-bearing F5-K5 stars as they are around the A-F stars first detected by IRAS.

Our finding is in contrast with Greaves et al. (2004), who found no overlap between stars with disks and stars with planets. In order to look for dust/planet systems, they observed a sample of 8 planet-bearing stars in the sub-mm, with no detections. The disks identified by *Spitzer*, however, are considerably less massive than those detectable in the submillimeter. For example, in the case of  $\epsilon$  Eri, the ratio of 60  $\mu\text{m}$  IRAS emission (1,600 mJy) to 850  $\mu\text{m}$  emission (40 mJy) is 40:1. If this same ratio applies to the sources seen here which have a typical 70  $\mu\text{m}$  brightness of 35 mJy, the predicted submillimeter flux density would be  $\sim 1$  mJy which is just the  $1\text{-}\sigma$  noise limit for the SCUBA survey. Six of the eight sub-mm sources are also in our target sample, allowing a direct comparison of *Spitzer* with SCUBA. In contrast with the sub-mm non-detections, five photospheres were observed with  $\text{SNR} \gtrsim 5$ , and one star (HD117176, 70 Vir) was found to have significant 70  $\mu\text{m}$  excess. While SCUBA follow-up observations of the sources detected here will be very important for constraining the temperature and total mass of dust, conclusions about the incidence of disks around planet-bearing stars require *Spitzer's* higher sensitivity.

While excesses at 70  $\mu\text{m}$  are relatively frequent in our survey, we find no evidence for excess at 24  $\mu\text{m}$  around any of the planet-bearing stars. The lack of 24  $\mu\text{m}$  emission in these systems is consistent with the previously known lack of warm material toward stars older than a few 100 Myr (Aumann & Probst 1991; Fajardo-Acosta et al. 2000; Laureijs et al. 2002). Assuming peak 24  $\mu\text{m}$  emission from 150 K dust and the observed dispersion ( $F_d/F_\star < 0.07$ ), we can set a  $3\text{-}\sigma$  upper limit on  $L_{\text{dust}}/L_\star$  for hotter dust of  $5 \times 10^{-5}$  which is well above the  $10^{-7}$  level of emission from our asteroid belt, but well below the level seen toward young A stars such as  $\beta$  Pic or Fomalhaut ( $\alpha$  PsA). As described above, the lack of warm material is consistent with its destruction or dispersal by the gravitational effect of planets in the 1-5 AU region (Liou & Zook 1999).

For stars with a single measurement of excess at 70  $\mu\text{m}$ , the dust properties are not well constrained, but are generally consistent with Kuiper belt configurations - distances of several tens of AU and temperatures  $\sim 50$  K. The observed dust luminosities (relative to the central stars'), however, are much brighter, exceeding the Kuiper belt's  $L_{\text{dust}}/L_\star$  by factors of  $\sim 100$ .

Within the planet-bearing sample there is little to no correlation of 70  $\mu\text{m}$  excess with stellar age, metallicity, or spectral type. But there is a strong hint of a positive correlation between both the frequency and the magnitude of dust emission with the presence of known planets. As more *Spitzer* observations of planet-bearing and non-planet-bearing stars are made, as part of this survey and in other programs, these statistics will become much better defined. Additional radial velocity studies of stars with excesses but without presently known planets will test the predictive power of this correlation.

We would like to thank Debra Fischer and Geoff Marcy for discussions on stellar metallicity, updates on RV planet searches, and commentary on  $\epsilon$  Eri’s variability. This publication makes use of data products from the Two Micron All Sky Survey (2MASS), as well as from IPAC/ibis, SIMBAD, and VIZIER; Samantha Lawler assisted in the compilation of data from these sources. We acknowledge technical support from the Center for Long-Wavelength Astrophysics at JPL, particularly from J. Arballo and T. Thompson.

The *Spitzer Space Telescope* is operated by the Jet Propulsion Laboratory, California Institute of Technology, under NASA contract 1407. Development of MIPS was funded by NASA through the Jet Propulsion Laboratory, subcontract 960785. Some of the research described in this publication was carried out at the Jet Propulsion Laboratory, California Institute of Technology, under a contract with the National Aeronautics and Space Administration.

Finally, we note that much of the preparation for the observations described here was carried out by Elizabeth Holmes, who passed away in March 2004. This work is dedicated to her memory.

## REFERENCES

- Aumann, H. H. & Good, J. C. 1990, *ApJ*, 350, 408
- Aumann, H. H. & Probst, R. G. 1991, *ApJ*, 368, 264
- Backman, D. E. & Paresce, F. 1993, in *Protostars and Planets III*, 1253–1304
- Baglin, A., Auvergne, M., Barge, P., et al. 2002, in *ESA SP-485: Stellar Structure and Habitable Planet Finding*, 17–24
- Beichman, C. A., et al. 2005, *ApJ*, in preparation
- Bryden, G., Lin, D. N. C., & Ida, S. 2000, *ApJ*, 544, 481
- Bryden, G., et al. 2005, *ApJ*, in preparation
- Campbell, B., Walker, G. A. H., & Yang, S. 1988, *ApJ*, 331, 902
- Castelli, F. 2003, in *IAU Symposium*, 47
- Cohen, M., Walker, R. G., Carter, B., et al. 1999, *AJ*, 117, 1864
- Cumming, A., Marcy, G. W., & Butler, R. P. 1999, *ApJ*, 526, 890



- Decin, G., Dominik, C., Malfait, K., Mayor, M., & Waelkens, C. 2000, *A&A*, 357, 533
- Decin, G., Dominik, C., Waters, L. B. F. M., & Waelkens, C. 2003, *ApJ*, 598, 636
- Dermott, S. F., Durda, D. D., Grogan, K., & Kehoe, T. J. J. 2002, *Asteroids III*, 423
- Dole, H., Le Floch, E., Pérez-González, P. G., et al. 2004a, *ApJS*, 154, 87
- Dole, H., Rieke, G. H., Lagache, G., et al. 2004b, *ApJS*, 154, 93
- Dominik, C. & Decin, G. 2003, *ApJ*, 598, 626
- Dominik, C., Laureijs, R. J., Jourdain de Muizon, M., & Habing, H. J. 1998, *A&A*, 329, L53
- Draine, B. T. & Lee, H. M. 1984, *ApJ*, 285, 89
- Engelke, C. W. 1992, *AJ*, 104, 1248
- Fajardo-Acosta, S. B., Beichman, C. A., & Cutri, R. M. 2000, *ApJ*, 538, L155
- Fischer, D. A. & Valenti, J. A. 2003, in *ASP Conf. Ser. 294: Scientific Frontiers in Research on Extrasolar Planets*, 117–128
- Gillett, F. C. 1986, in *ASSL Vol. 124: Light on Dark Matter*, 61–69
- Gordon, K. D., et al. 2004a, *PASP*, submitted
- . 2004b, *SPIE*, 5487, in press
- Greaves, J. S., Holland, W. S., Jayawardhana, R., Wyatt, M. C., & Dent, W. R. F. 2004, *MNRAS*, 348, 1097
- Greaves, J. S., Holland, W. S., Moriarty-Schieven, G., et al. 1998, *ApJ*, 506, L133
- Habing, H. J., Dominik, C., Jourdain de Muizon, M., et al. 2001, *A&A*, 365, 545
- Hatzes, A. P., Cochran, W. D., McArthur, B., et al. 2000, *ApJ*, 544, L145
- Heap, S. R., Lindler, D. J., Lanz, T. M., et al. 2000, *ApJ*, 539, 435
- Holland, W. S., Greaves, J. S., Dent, W. R. F., et al. 2003, *ApJ*, 582, 1141
- Holland, W. S., Greaves, J. S., Zuckerman, B., et al. 1998, *Nature*, 392, 788
- IPAC. 1994, *IRAS Sky Survey Atlas (ISSA)* (Pasadena: Jet Propulsion Laboratory (IPAC), 1992 /—c1994)

- Israelian, G., Santos, N. C., Mayor, M., & Rebolo, R. 2001, *Nature*, 411, 163
- . 2003, *A&A*, 405, 753
- Jayawardhana, R., Holland, W. S., Kalas, P., et al. 2002, *ApJ*, 570, L93
- King, J. R., Villarreal, A. R., Soderblom, D. R., Gulliver, A. F., & Adelman, S. J. 2003, *AJ*, 125, 1980
- Kurucz, R. L. 2003, in *IAU Symposium*, 45
- Lagache, G., Dole, H., Puget, J.-L., et al. 2004, *ApJS*, 154, 112
- Laureijs, R. J., Jourdain de Muizon, M., Leech, K., et al. 2002, *A&A*, 387, 285
- Liou, J. & Zook, H. A. 1999, *AJ*, 118, 580
- Marcy, G. W. & Butler, R. P. 1995, *Bulletin of the American Astronomical Society*, 27, 1379
- Mayor, M. & Queloz, D. 1995, *Nature*, 378, 355
- Moro-Martin, A. & Malhotra, R. 2005, in *The Dusty and Molecular Universe: A Prelude to Herschel and ALMA*, meeting held in Paris, France, October 27-29, 2004, Eds.: A. Wilson. To be published in *ESA Conference Series.*, p.296
- Moshir, M., et al. 1990, in *IRAS Faint Source Catalogue*, version 2.0
- Plets, H. & Vynckier, C. 1999, *A&A*, 343, 496
- Rieke, G. H., Young, E. T., Engelbracht, C. W., et al. 2004, *ApJS*, 154, 25
- Rieke, G. H., Su, K. Y. L., Stansberry, J. A., Trilling, D., Bryden, G., Muzerolle, J., White, B., Gorlova, N., Young, E. T., Beichman, C. A., Stapelfeldt, K. R., & Hines, D. C. 2004, *ApJ*, in press
- Schneider, G., Becklin, E. E., Smith, B. A., et al. 2001, *AJ*, 121, 525
- Schneider, G., Smith, B. A., Becklin, E. E., et al. 1999, *ApJ*, 513, L127
- Sheret, I., Dent, W. R. F., & Wyatt, M. C. 2004, *MNRAS*, 348, 1282
- Skrutskie, M. F., Schneider, S. E., Stiening, R., et al. 2000, *VizieR Online Data Catalog*, 2241
- Spangler, C., Sargent, A. I., Silverstone, M. D., Becklin, E. E., & Zuckerman, B. 2001, *ApJ*, 555, 932

- Stapelfeldt, K. R., Holmes, E. K., Chen, C., et al. 2004, *ApJS*, 154, 458
- Stern, S. A. 1996, *A&A*, 310, 999
- Teplitz, V. L., Stern, S. A., Anderson, J. D., et al. 1999, *ApJ*, 516, 425
- Tobiska, W. K., Woods, T., Eparvier, F., et al. 2000, *Journal of Atmospheric and Terrestrial Physics*, 62, 1233
- Trilling, D. E., Brown, R. H., & Rivkin, A. S. 2000, *ApJ*, 529, 499
- Werner, M. W., Roellig, T. L., Low, F. J., et al. 2004, *ApJS*, 154, 1
- Wright, J. T., Marcy, G. W., Butler, R. P., & Vogt, S. S. 2004, *ApJS*, 152, 261
- Wyatt, M. C. & Dent, W. R. F. 2002, *MNRAS*, 334, 589

HD #	name	$M_p \sin i$ ( $M_{\text{Jup}}$ )	$a_p$ (AU)	$e_p$
142	GJ4.2A	1.36	0.98	0.37
1237	GJ 3021	3.21	0.49	0.505
13445	Gl 86	4	0.11	0.046
17051	$\iota$ Hor, HR 810	2.26	0.925	0.161
27442	GJ167.3	1.28	1.18	0.07
33636*	BD+04858	9.28	3.56	0.53
39091	GJ 9189	10.35	3.29	0.62
50554*	BD+241451	4.9	2.38	0.42
52265*	HR 2622	1.13	0.49	0.29
75732	55 ( $\rho$ ) Cnc	0.045	0.038	0.174
		0.84	0.11	0.02
		0.21	0.24	0.34
		4.05	5.9	0.16
82943*	BD-112670	0.88	0.73	0.54
		1.63	1.16	0.41
95128	47 Uma	2.41	2.1	0.096
		0.76	3.73	< 0.1
114783	GJ 3769	0.9	1.2	0.1
117176*	70 Vir	7.44	0.48	0.4
120136	$\tau$ Boo, GJ 527A	3.87	0.0462	0.018
128311*	GJ 3860	2.63	1.06	0.21
134987	23 Lib	1.58	0.78	0.25
143761	$\rho$ CrB	1.04	0.22	0.04
145675	14 Her	4.89	2.85	0.38
160691	$\mu$ Arae, GJ 691	0.042	0.09	0
		1.7	1.5	0.31
		3.1	4.17	0.8
168443	GJ 4052	7.7	0.29	0.529
		16.9	2.85	0.228
169830	HR 6907	2.88	0.81	0.31
		4.04	3.6	0.33
177830	GJ 743.2	1.28	1	0.43
186427	16 Cyg B	1.69	1.67	0.67
210277	GJ 848.4	1.28	1.097	0.45
216437	$\rho$ Ind	2.1	2.7	0.34

\*star with excess 70  $\mu\text{m}$  emission

Table 1: Orbital characteristics of the known planets surrounding stars observed by Spitzer. Also see Fig 6 for a graphical display of some of this information.

HD #	24 $\mu\text{m}$			70 $\mu\text{m}$						
	$F_{\text{MIPS}}$	$F_{\star}$	$F_{\text{MIPS}}/F_{\star}$	$F_{\text{MIPS}}$	$F_{\star}$	$F_{\text{MIPS}}/F_{\star}$	SNR	$\chi_{70}$	$F_{\text{dust}}^{\dagger}$	$L_{\text{dust}}/L_{\star}$
142	117.3	123.3	0.95	$26.4 \pm 5.1$	13.9	1.9	5.6	2.4		$<2.0 \times 10^{-5}$
1237	82.9	88.7	0.94	$10.0 \pm 2.9$	10.1	1.0	4.0	0.0		$<9.0 \times 10^{-6}$
13445	162.9	166.9	0.98	$3.9 \pm 6.3$	19.0	0.2	0.7	-2.4		$<4.1 \times 10^{-6}$
17051	166.8	161.7	1.03	$20.1 \pm 4.1$	18.1	1.1	6.4	0.5		$<6.7 \times 10^{-6}$
27442	1147.7	1222.7	0.94	$126.5 \pm 21.9$	139	0.9	19.2	-0.6		$<7.8 \times 10^{-6}$
33636*	42.9	44.1	0.97	$33.1 \pm 2.3$	5.0	6.7	15.4	12.4	32.4	$4.9 \times 10^{-5}$
39091	139.9	150.4	0.93	$21.5 \pm 3.6$	17.0	1.3	8.3	1.3		$<9.0 \times 10^{-6}$
50554*	47.1	51.2	0.92	$39.5 \pm 2.8$	5.8	6.8	14.9	12.1	38.8	$4.4 \times 10^{-5}$
52265*	74.3	70.7	1.05	$31.7 \pm 7.4$	8.0	4.0	4.3	3.2	27.3	$2.9 \times 10^{-5}$
75732	172.8	162.7	1.06	$18.9 \pm 4.5$	18.2	1.0	5.3	0.2		$<8.3 \times 10^{-6}$
82943*	66.5	66.5	1.00	$113.3 \pm 6.8$	7.5	15.1	17.0	15.7	122	$1.2 \times 10^{-4}$
95128	259.5	265.9	0.98	$29.1 \pm 6.0$	30	1.0	7.3	-0.1		$<4.8 \times 10^{-6}$
114783	45.2	52.1	0.87	$6.2 \pm 2.2$	6.0	1.0	3.2	0.1		$<1.4 \times 10^{-5}$
117176*	373.6	395	0.95	$77.4 \pm 10.2$	44.8	1.7	10.2	3.2	37.6	$1.0 \times 10^{-5}$
120136	338.2	321.7	1.05	$30.9 \pm 7.9$	36.3	0.9	5.4	-0.7		$<3.7 \times 10^{-6}$
128311*	67 <sup>‡</sup>	73.5	0.91	$26.5 \pm 3.9$	8.4	3.2	7.1	4.6	20.8	$3.0 \times 10^{-5}$
134987	78.8	68.3	1.15	$3.1 \pm 4.5$	7.7	0.4	0.7	-1.0		$<1.1 \times 10^{-5}$
143761	201.8	192.5	1.05	$27.8 \pm 6.1$	21.7	1.3	5.4	1.0		$<9.6 \times 10^{-6}$
145675	92.4	106.4	0.87	$9.2 \pm 2.5$	12	0.8	5.4	-1.1		$<4.8 \times 10^{-6}$
160691	270.6	273.5	0.99	$24.1 \pm 8.5$	30.8	0.8	3.4	-0.8		$<6.1 \times 10^{-6}$
168443	55.6	53.3	1.04	$9.6 \pm 29.6^{\diamond}$	6.0	1.6	0.3	0.1		$<1.5 \times 10^{-4}$
169830	99.0	104.8	0.94	$4.7 \pm 5.9$	11.9	0.4	0.8	-1.2		$<6.5 \times 10^{-6}$
177830	88.6	104.3	0.85	$4.4 \pm 3.5$	11.8	0.4	1.5	-2.1		$<3.2 \times 10^{-6}$
186427	93.0	103.1	0.90	$3.0 \pm 5.6$	11.6	0.3	0.5	-1.5		$<4.3 \times 10^{-6}$
210277	83.5	91.9	0.91	$8.0 \pm 2.9$	10.4	0.8	3.2	-0.8		$<5.1 \times 10^{-6}$
216437	107.5	102.1	1.05	$9.5 \pm 3.9$	11.5	0.8	2.7	-0.5		$<8.4 \times 10^{-6}$

\*star with excess 70  $\mu\text{m}$  emission

<sup>†</sup>dust fluxes have been color corrected by 15%, appropriate for  $\sim 50\text{K}$  emission

<sup>‡</sup>24  $\mu\text{m}$  flux is from IRAS 25  $\mu\text{m}$

<sup>◊</sup>high galactic cirrus contamination

Table 2: Measured and predicted fluxes at 24 and 70  $\mu\text{m}$  for the planet-bearing stars, in mJy. For the 70  $\mu\text{m}$  data, we also list the signal-to-noise ratio (SNR), the significance level of any excess ( $\chi_{70}$ ; see Eq 1), and  $L_{\text{dust}}/L_{\star}$ , the minimum disk luminosity (see Eq 3 in §4).

HD #	Spectral Type	[Fe/H]	dist. (pc)	age (Gyr)
142	G1 IV	0.02	25.64	2.9
1237	G6 V	0.10	17.62	2.8
13445	K1 V	-0.19	10.95	5.6
17051	G0 V	0.09	17.24	2.4
27442	K2 IVa	0.21	18.23	6.6
33636*	G0	-0.13	28.69	3.2
39091	G1 V	0.11	18.21	5.6
50554*	F8	-0.05	31.03	4.7
52265*	G0	0.20	28.07	6.0
75732	G8 V	0.31	12.53	6.5
82943*	G0	0.27	27.46	4.1
95128	G0 V	-0.02	13.91	6.0
114783	K0 V	-0.13	20.43	4.4
117176*	G2.5Va	-0.06	18.11	5.4
120136	F7 V	0.24	13.51	1.9
128311*	K0	0.08	16.57	0.5 <sup>†</sup>
134987	G5 V	0.28	25.65	7.8
143761	G0 V	-0.23	17.43	7.4
145675	K0 V	0.41	18.15	6.9
160691	G3 IV-V	0.29	15.28	6.7
168443	G5 V	-0.01	37.88	8.5
169830	F8	0.14	36.32	7.2
177830	K0	0.36	59.03	8.5
186427	G3 V	0.06	21.41	7.4
210277	G0V	0.23	21.29	6.8
216437	G2.5IV	0.20	26.52	7.2

\*star with excess 70  $\mu\text{m}$  emission

<sup>†</sup>see discussion of HD128311's age in §3.2

Table 3: Spectral type, metallicity, distance, and age for planet-bearing stars observed by Spitzer.

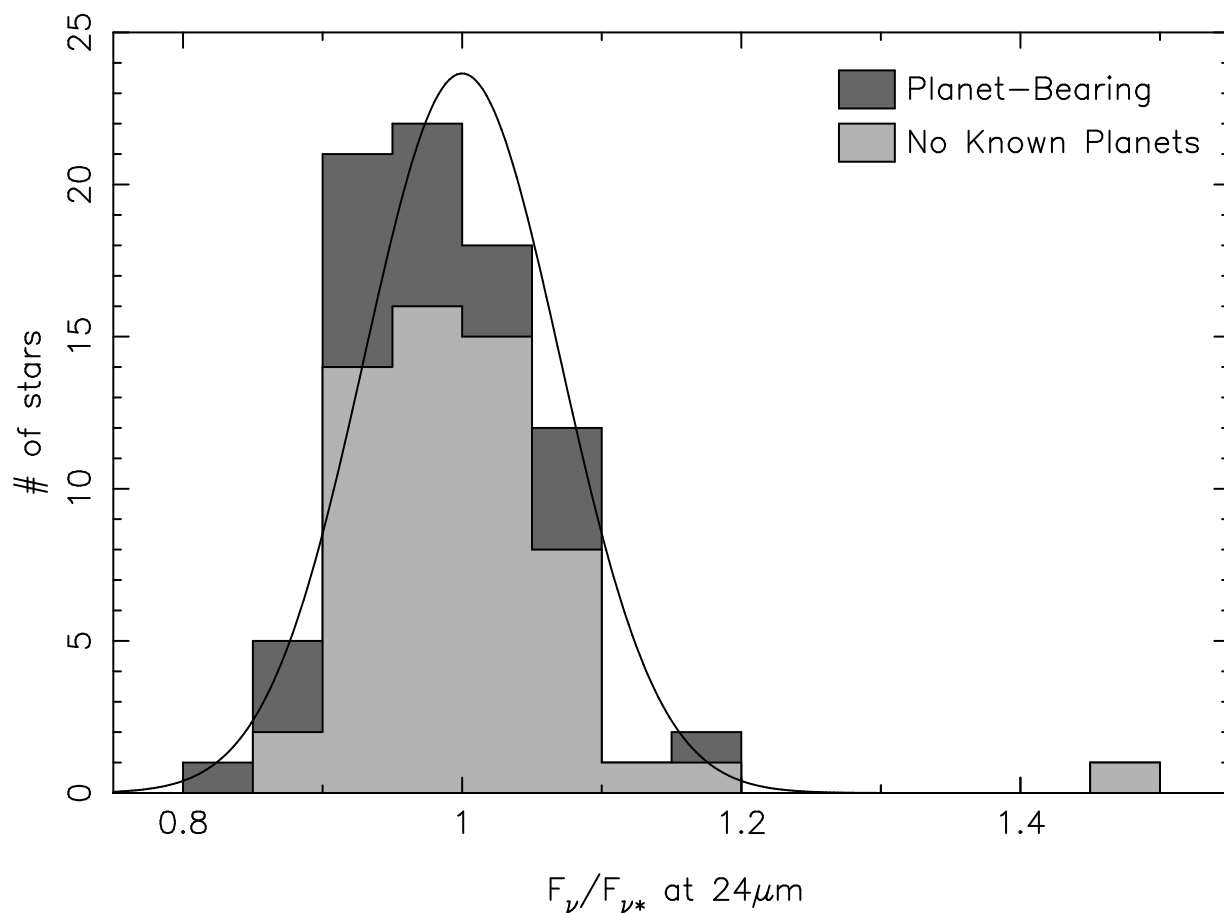


Fig. 1.— Distribution of  $24 \mu\text{m}$  fluxes relative to the expected photospheric values for a sample of 84 stars. A gaussian distribution with dispersion 0.07 is shown for comparison. One star (HD69830; Beichman et al. 2005) clearly stands out from the main population of stars with no excess emission above their stellar photospheres. In this histogram and those that follow, stars with planets are shaded with dark grey while stars without known planets are designated by light grey.

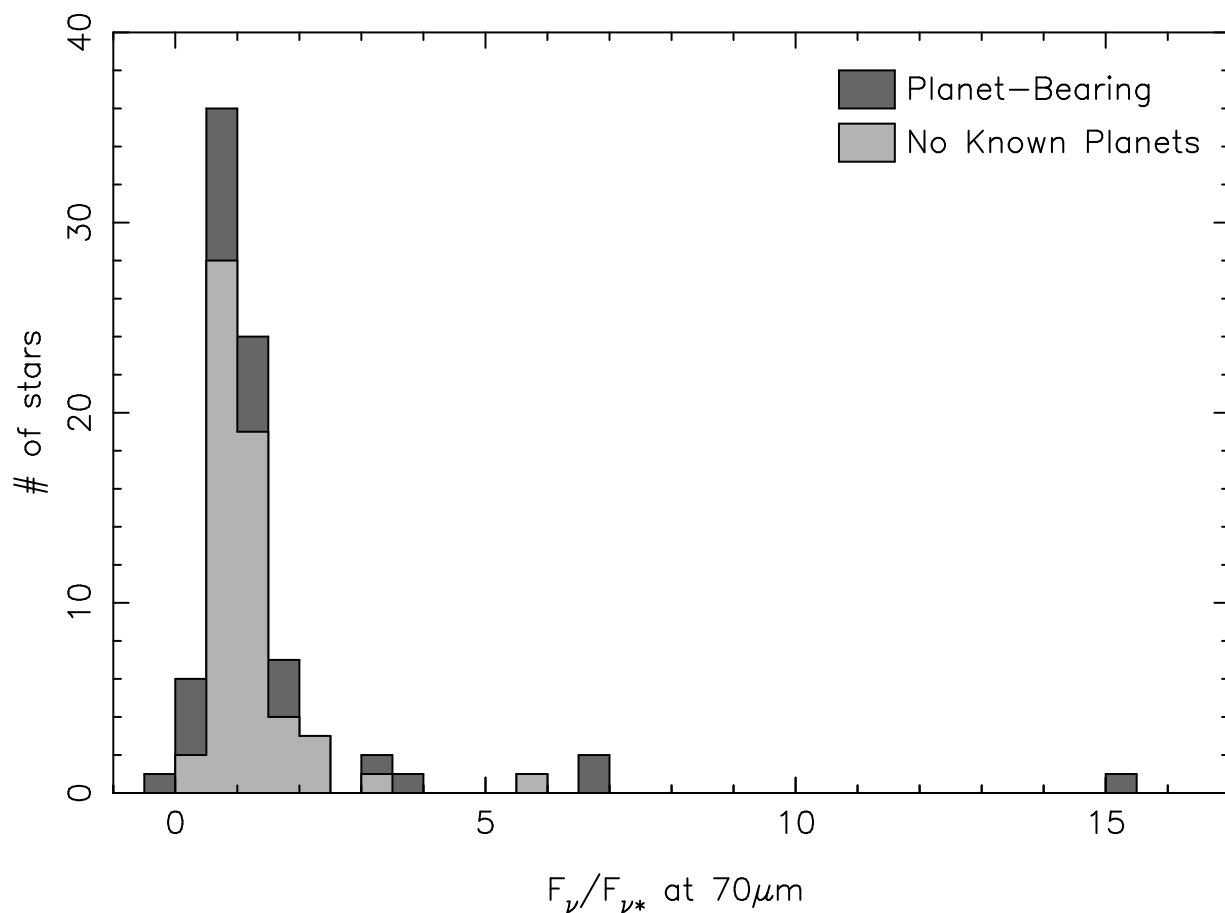


Fig. 2.— Distribution of  $70\ \mu\text{m}$  fluxes relative to the expected photospheric values for a sample of 84 stars. While most stars cluster around 1, where their flux is photospheric, several stars show a high degree of excess emission. Stars with planets are shaded as dark grey while stars without known planets are designated with light grey. Although planet-bearing stars make up less than a third of the sample, four out of the five stars with the highest factor of excess  $70\ \mu\text{m}$  emission are known to have planets.



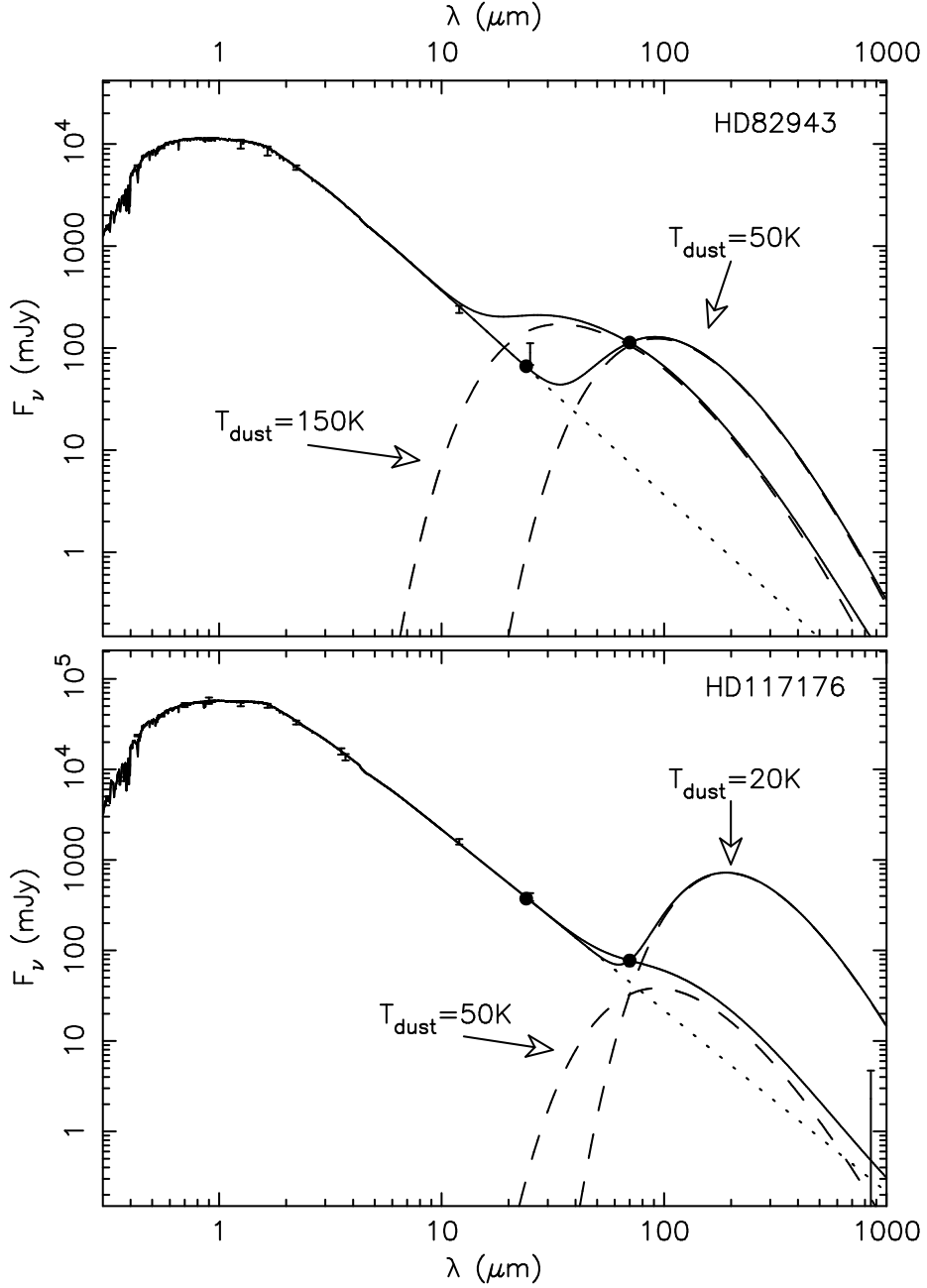


Fig. 3.— Spectral energy distributions for HD82943 and HD117176. In addition to our 24 and 70  $\mu\text{m}$  *Spitzer* data (dark circles), we also show optical measurements and IRAS fluxes at 12 and 25  $\mu\text{m}$ . For HD117176, a sub-mm (850  $\mu\text{m}$ ) constraint is also available (Greaves et al. 2004). The emission from dust at a given temperature (dashed lines) is added to the stellar Kurucz model (dotted line) in order to fit the observed excess emission at 70  $\mu\text{m}$ . In each plot, two separate fits (two different dust temperatures) are considered. In the case of HD82943 hot dust (150 K) is ruled out by the 24  $\mu\text{m}$  observations, while for HD117176 cold dust (20 K) is excluded by the sub-mm upper limit (see §4 for discussion of the limits on dust temperature and luminosity).

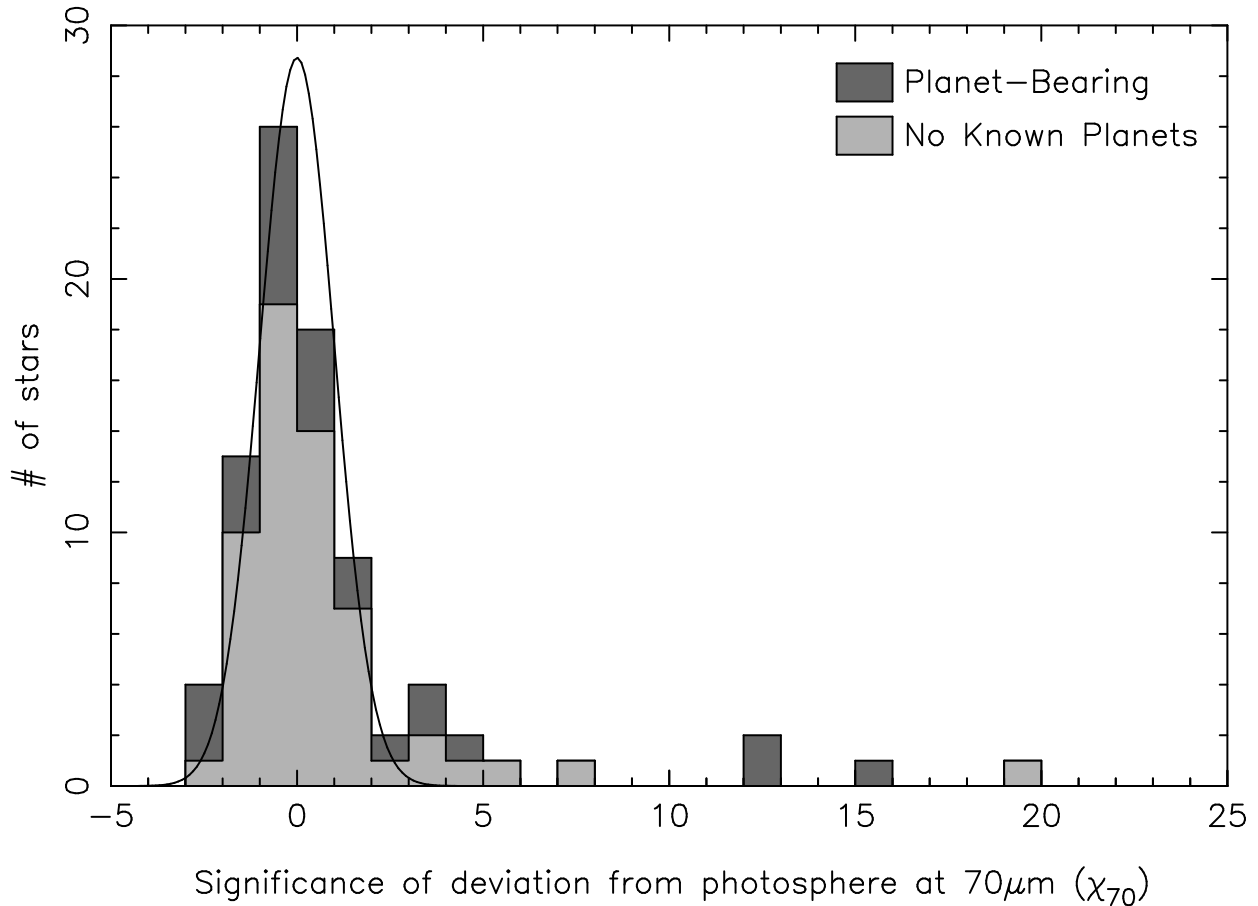


Fig. 4.— Statistical significance of deviations from the expected stellar flux at  $70 \mu\text{m}$ . A gaussian distribution of errors is shown for comparison. In order to be considered a significant  $70 \mu\text{m}$  excess,  $\chi_{70}$  should at least exceed the  $3\text{-}\sigma$  level. Six of the stars with planets (dark grey) meet this criterion, as do six of the stars without known planets (light grey).

Fig. 5.—  $70 \mu\text{m}$  images for the six planet-bearing stars with excess emission. The contrast scale is the same for each image. The images are  $\sim 2$  arcmin on each side; the beam size fwhm is  $17''$ . North is oriented upward and east to the left within each frame.

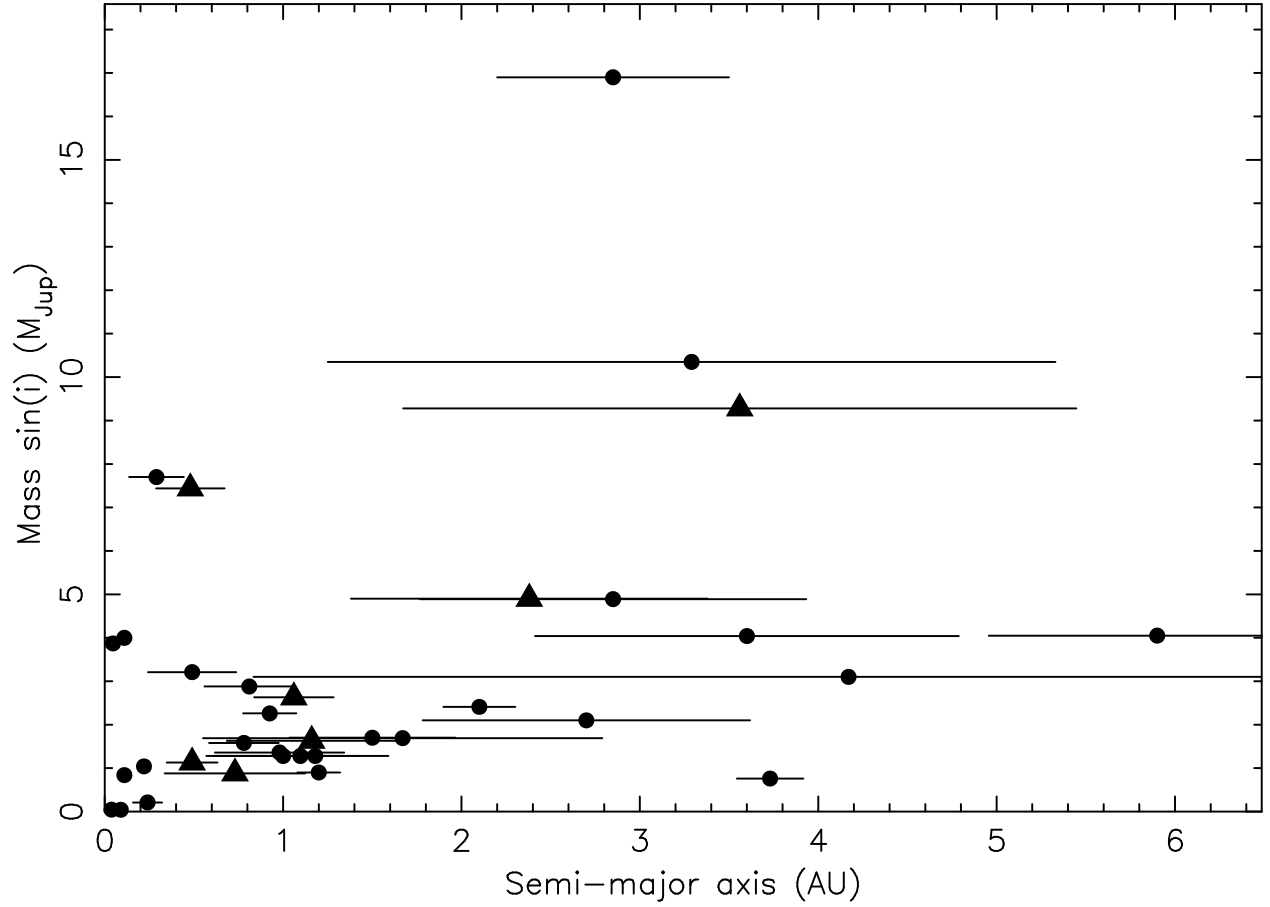


Fig. 6.— Orbital characteristics for the survey stars. Minimum planet mass ( $M_p \sin i$ ) is plotted versus each planet’s semi-major axis ( $a_p$ ). The lines extend from periaapse ( $a_p(1 - e_p)$ ) to apoapse ( $a_p(1 + e_p)$ ). The planets which are associated with  $70 \mu\text{m}$  excess are marked as triangles, while those without are circles.

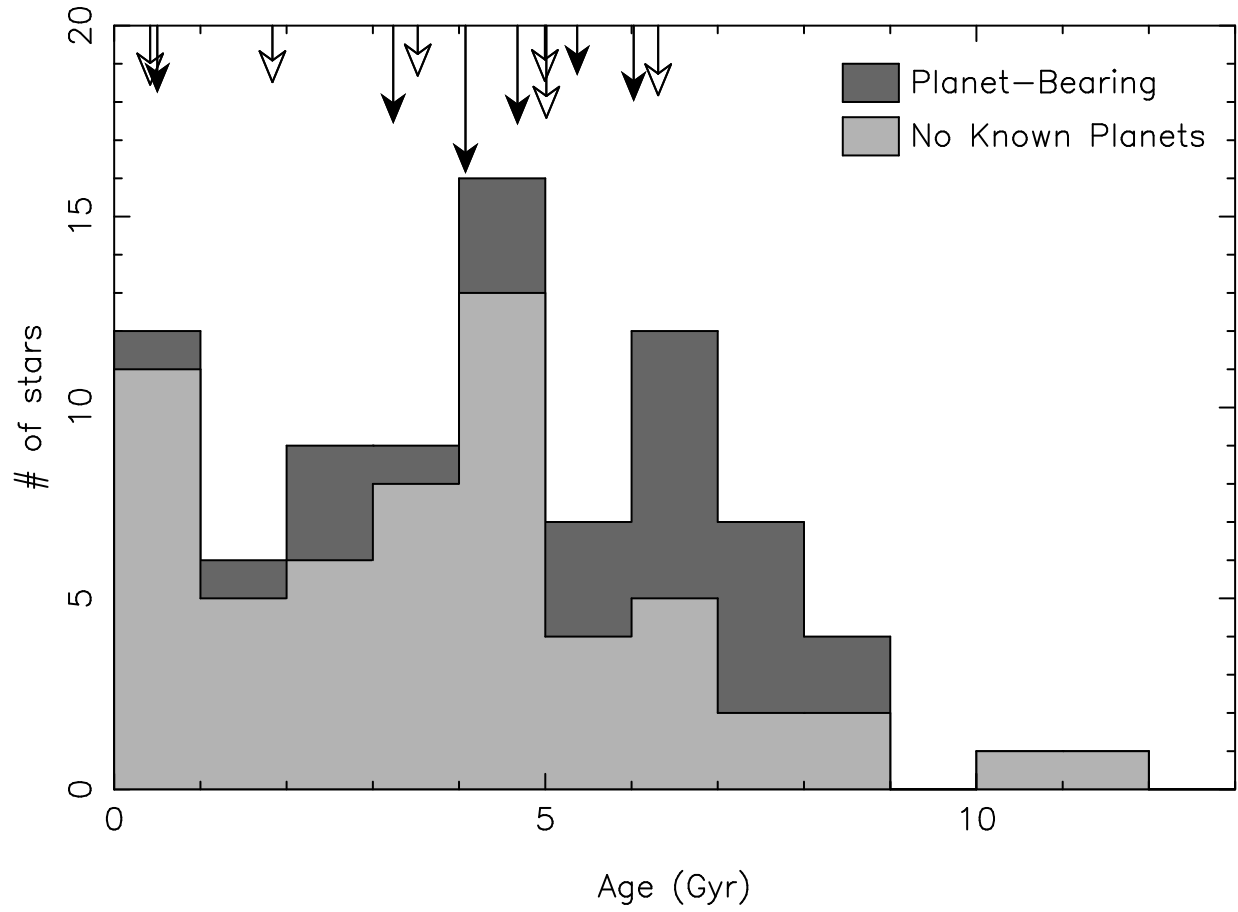


Fig. 7.— Distribution of stellar ages. Stars with planets are shaded as dark grey while stars without known planets are designated with light grey. The ages of stars with  $70 \mu\text{m}$  excess are flagged as arrows at the top of the plot. For planet-bearing stars the arrows are filled; for stars without known planets they are open. The length of the arrow is an indicator of the strength of  $70 \mu\text{m}$  excess.

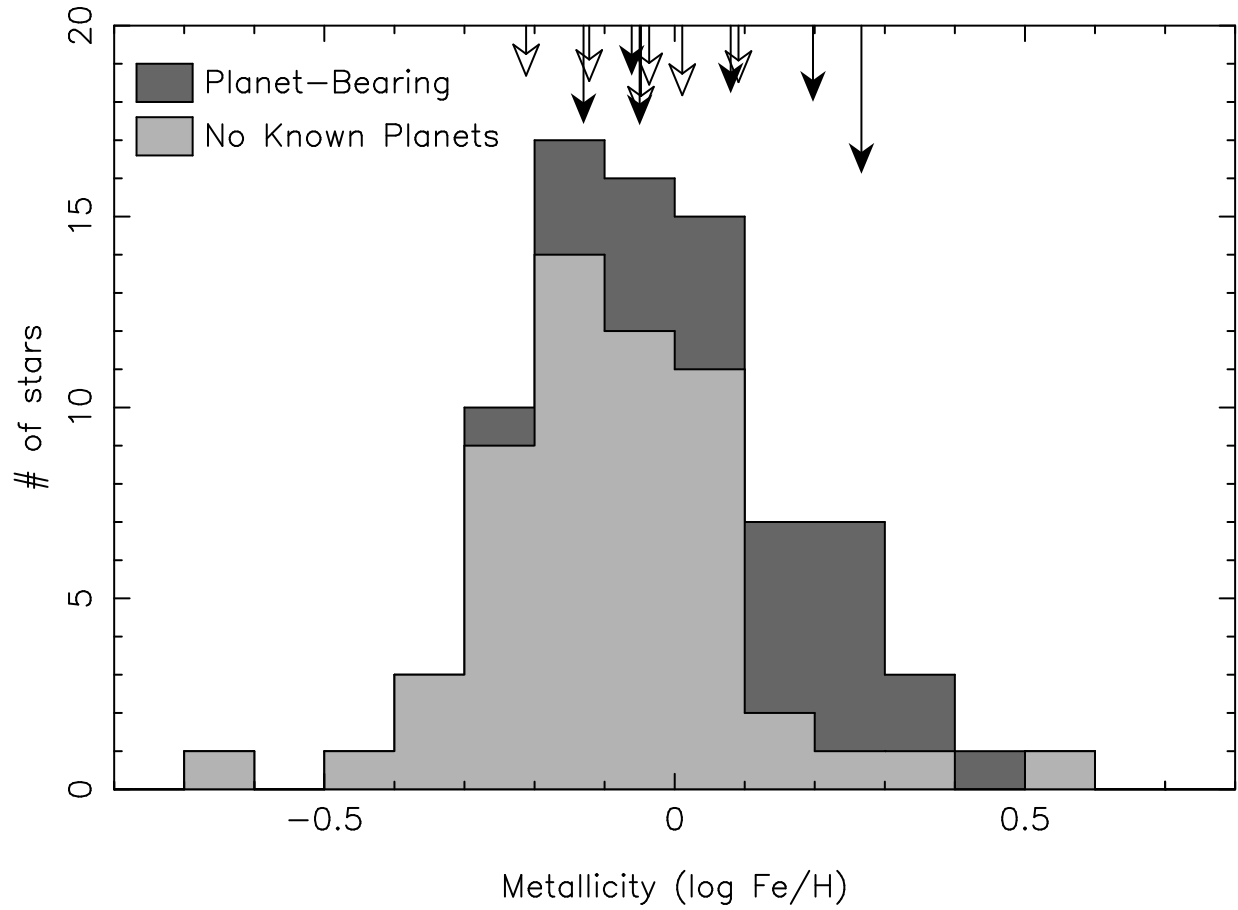


Fig. 8.— Distribution of stellar metallicities. Stars with planets are shaded as dark grey while stars without known planets are designated with light grey. The metallicities of stars with 70  $\mu\text{m}$  excess are flagged as arrows at the top of the plot. For planet-bearing stars the arrows are filled; for stars without known planets they are open. The length of the arrow is an indicator of the strength of 70  $\mu\text{m}$  excess.

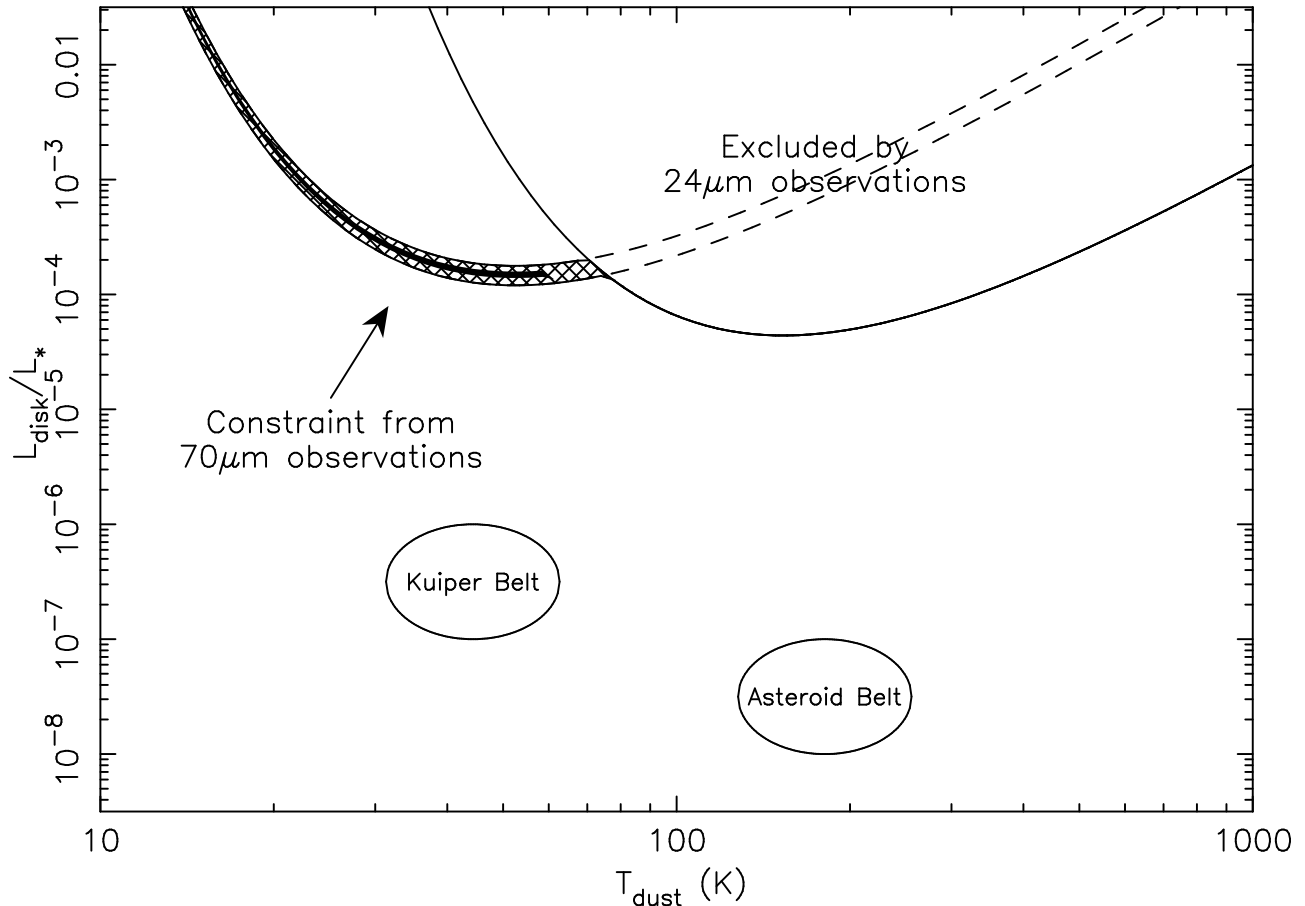


Fig. 9.— Constraints on the temperature and total luminosity of the dust around HD82943, as provided by 24 and 70  $\mu\text{m}$  MIPS observations. The area to the upper right (hot temperature, bright luminosity) is ruled out by the 24  $\mu\text{m}$  upper limit on the dust emission. The 3- $\sigma$  limits around 70  $\mu\text{m}$  detection confine the dust characteristics within the cross-hatched region. The solid-filled region is defined by 1- $\sigma$  error limits. Without any longer wavelength information, there is no lower limit on the dust temperature or upper limit on the dust luminosity. The approximate characteristics of the asteroid and Kuiper belts are shown for comparison.

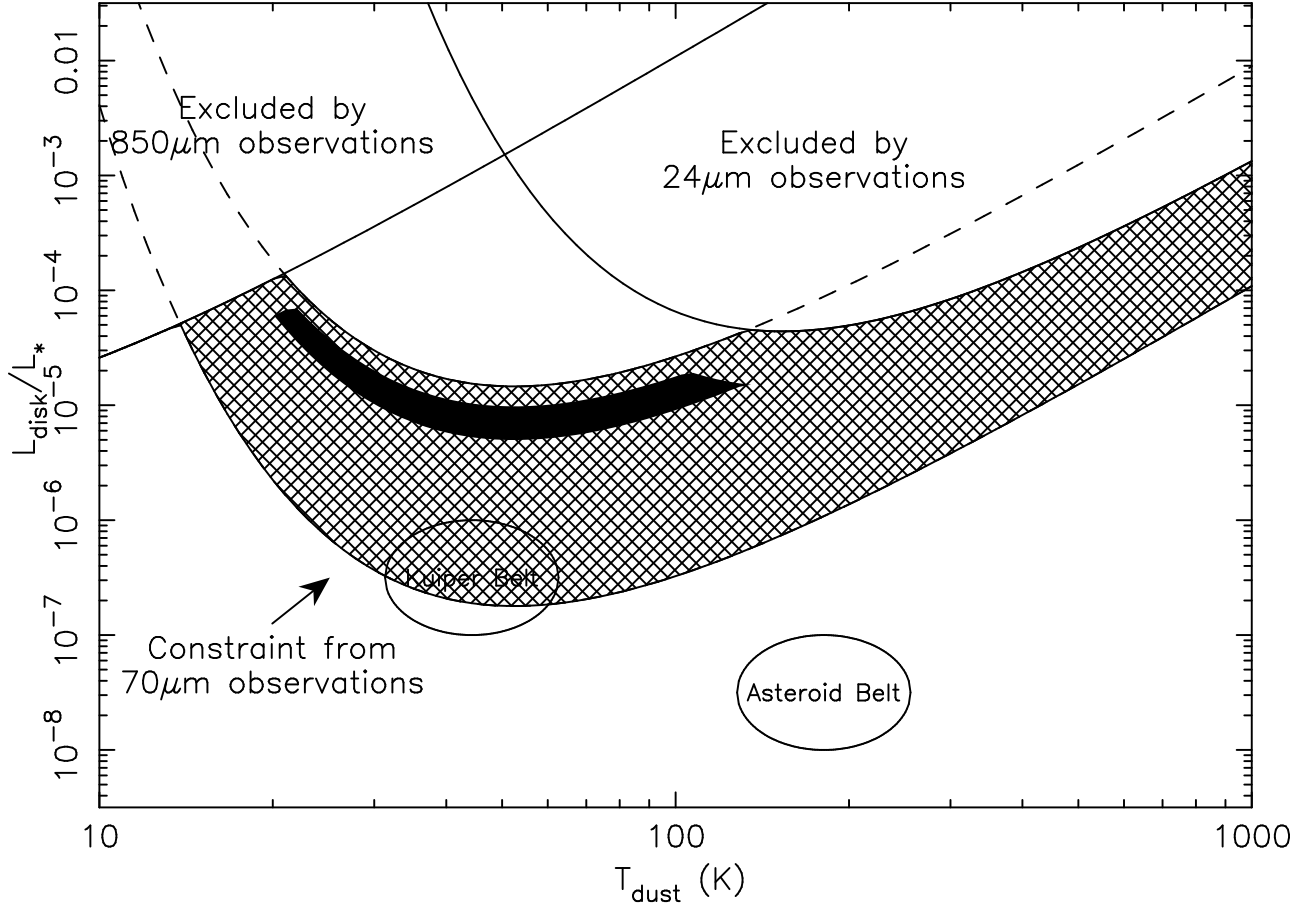


Fig. 10.— Constraints on the temperature and total luminosity of the dust around HD117176, as provided by 24 and 70  $\mu\text{m}$  MIPS data combined with sub-mm observations. The upper right is ruled out by the 24  $\mu\text{m}$  upper limit, while the upper left is ruled out by the sub-mm (Greaves et al. 2004). Based on the 70  $\mu\text{m}$  data, the dust temperature and luminosity are confined to the shaded region. The 3- $\sigma$  limits for the three wavelengths confine the dust characteristics within the cross-hatched region, while the solid-filled region is defined by 1- $\sigma$  error limits. Again, the approximate characteristics of the asteroid and Kuiper belts are shown for comparison. Note that although the formal 3- $\sigma$  error limits extend as low as the Kuiper belt’s luminosity, the Kuiper belt itself would be too faint to detect.